First Measurements of the Nitrogen Stable Isotope Composition ($\delta^{15}N$) of Ship-emitted NO_x

Zeyu Sun[1,2,8], Zheng Zong[1,3], Yang Tan[1], Chongguo Tian[1,2,7,*], Zeyu Liu[4], Fan Zhang[5], Rong Sun[1,2], Yingjun Chen[4], Jun Li[6], Gan Zhang[6]

[1]CAS Key Laboratory of Coastal Environmental Processes and Ecological Remediation, Yantai Institute of Coastal Zone Research, Chinese Academy of Sciences, Yantai, 264003, China

[2]Shandong Key Laboratory of Coastal Environmental Processes, Yantai, 264003, China

[3]Department of Civil and Environmental Engineering, Hong Kong Polytechnic University, Hong Kong, 999077, China

[4]Shanghai Key Laboratory of Atmospheric Particle Pollution and Prevention (LAP3), Department of Environmental Science and Engineering, Fudan University, Shanghai, China

[5]Key Lab of Geographic Information Science of the Ministry of Education, School of Geographic Sciences, East China Normal University, Shanghai, 210062, China

[6]State Key Laboratory of Organic Geochemistry and Guangdong Key Laboratory of Environmental Protection and Resources Utilization, Guangzhou Institute of Geochemistry, Chinese Academy of Sciences, Guangzhou, 510640, China

[7]Center for Ocean Mega–Science, Chinese Academy of Sciences, Qingdao, 266071, China

[8]University of Chinese Academy of Sciences, Beijing, 100049, China

Correspondence to: Chongguo Tian (cgtian@yic.ac.cn)

The supplemental material has 22 pages and includes the following items:

Text S1. The principles and algorithm of methods implemented to evaluate the impact of different factors on the variation in ship-emitted $\delta^{15}N$–NO_x values

Text S2. The influence evaluation of the ship fuel type, the ship category, and the actual operational status of ships

Text S3. Significance of ship-emitted $\delta^{15}N$–NO_x values for accurate source apportionment of NO_x

Table S1. Technical parameters of the test ships

Table S2. Meteorological parameters during ship exhaust sampling (average values)

Table S3. Details on NO_x concentrations and $\delta^{15}N$–NO_x values for collected ship

Table S4. Statistics of $\delta^{15}N$–NO_x values and ranges of variation for emissions from other sources

Table S5. Results of variance analysis

Table S6. The accuracy of methods implemented to evaluate the impact degree of different factors on the variation in ship-emitted $\delta^{15}N$–NO_x values

Text S1. The principles and algorithm of methods implemented to evaluate the impact of different factors on the variation in ship-emitted $\delta^{15}N–NO_x$ values

In this study, the determination of whether each factor would have an effect on the nitrogen stable isotope composition ($\delta^{15}N$) values of nitrogen oxides (NO_x) from ships was achieved by the Kruskal–Wallis test, which is a nonparametric simulation similar to the one-way analysis of variance (ANOVA).(Kruskal and Wallis, 1952) The original hypothesis in Kruskal–Wallis test is that each sample obeys a probability distribution with the same median and rejection of the original hypothesis implies that at least one sample has a probability distribution with a median different from the others. Therefore, the Kruskal–Wallis test can estimate whether more than two independent samples come from the same probability distribution, but cannot identify between which samples these differences occur and the magnitude of the differences. Furthermore, the Mann–Whitney U test was used to determine whether there was a noticeable discrepancy between each pair of groups of ship-emitted $\delta^{15}N–NO_x$ values after division by each factor. Assuming that the two samples are from two aggregates that are identical except for the overall mean, the aim of this test is to conclude whether the means of these two aggregates are significantly different. With the Mann–Whitney U test, we can clearly determine at which stage of the changing influence factor the greatest difference in ship-emitted $\delta^{15}N–NO_x$ values occurs.(Mann and Whitney, 1947)

Conditional inference trees (CIT) are nonparametric class of decision trees that apply recursive binary partitioning of dependent variables based on the value of correlations. Each node of a tree is represented by a vector of case weights that has nonzero elements when the corresponding observations are elements of the node and zero otherwise. At a split, the feature with the lowest p value from a permutation test is selected. With this approach, it is possible to address different scales of the features in a natural way. Furthermore, it allows for unbiased selection of the features because the feature is selected in one step and the best split is determined when the variable to split on has been selected.(Hothorn et al., 2006) Random forest (RF) is an ensemble of regression trees and was originally proposed to classify dichotomous-dependent variables. RF uses the variance reduction in prediction accuracy before and after permuting the variable averaged over all trees to evaluate the importance of the candidate predictors. Specifically, for every bootstrap sample, the tree is grown in step 3 by recursively splitting data into distinct subsets so that one parent node has two child nodes. Data are split so that the purity of the data, i.e., the separation of affected and unaffected subjects, in the child nodes is maximized. The standard

measure for determining the best splitting feature together with its cutpoint is the Gini index. Alternatives include the deviance, entropy-based information gain, or the area under the curve splitting criterion.(Strobl et al., 2007; Speybroeck, 2012) Boosted regression trees (BRT) combine the strengths of two algorithms: regression trees (models that relate a response to their predictors by recursive binary splits) and boosting (an adaptive method for combining many simple models to give improved predictive performance). A certain amount of data is randomly selected several times during the operation to analyze the degree of influence of the independent variable on the dependent variable, the remaining data are used to check the fitting results, and the mean value of the generated multiple regression tree is taken and output. The BRT method is more tolerant to covariance and nonnormality among predictors and less prone to overfitting, so it has higher prediction accuracy for new data.(Elith et al., 2008)

Figure S4 displays the resulting conditional inference trees for $\delta^{15}N$ values of vessel-emitted NO_x. It was found that stage was the most important splitting factor of the root node. Samples collected from ships classified as having implemented the implementation of the International Maritime Organization (IMO) Tier I, II, and III were separated to terminal node 2, and the mean ± standard deviation of $\delta^{15}N$–NO_x values in the left branch (−16.8 ± 9.50‰) was significantly higher than that in the right branch (−33.8 ± 1.83‰), indicating a strong impact of implementing Annex V to the Prevention of Pollution from Ships (MARPOL) 73/78 on these $\delta^{15}N$–NO_x values. Ships that meet IMO Tier I and II requirements mainly reduce NO_x emissions by optimizing engines and fuels, while ships that meet Tier III requirements are equipped with selective catalytic reduction (SCR) systems based on this. In the CIT analysis, stage was again used as the next splitting factor to separate the samples collected from vessels meeting Tier III requirements as node 3. The mean ± standard deviation of $\delta^{15}N$–NO_x values in node 3 (−7.93 ± 5.33‰) was significantly higher than that in the right terminal node of this branch (−18.3 ± 9.25‰), indicating that the SCR system is more effective than the optimization of engine structure and fuel for changing the $\delta^{15}N$–NO_x values emitted from vessels. Recent studies found that the emitted NO_x was enriched in ^{15}N relative to the thermally produced nitrogen monoxide (NO) when the SCR system was effectively operating because the lighter NO molecules preferentially decomposed to nitrogen (N_2).(Walters et al., 2015a; Walters et al., 2015b) Ship type, as the next splitting factor of the right branch, separated the samples from the bulk carriers and fishing boats (mean, 22.55 mg kg^{-1}) from the passenger ships and research ships (mean, 14.87 mg kg^{-1}). Fuel type was the last splitting variable, separating samples taken when the ships used residual oil and diesel as fuel. In general, the CIT analysis identified that stage is the

most important factor influencing the variation in $\delta^{15}N–NO_x$ values, followed by ship type and fuel type.

Text S2. The influence evaluation of the ship fuel type, the ship category, and the actual operational status of ships

The statistics of $\delta^{15}N–NO_x$ values classified according to the ship fuel type, the ship category, and the actual operational status of ships are illustrated in Figures S1–S3. The influence of ship category on ship-emitted $\delta^{15}N–NO_x$ values primarily concerns engine types of different ships. For high-power engines, complete combustion of fuel raises the combustion temperature and the mixing time of fuel and air in the engine cylinder is longer, while the high oxygen content is also a dominant factor in NO_x generation.(Zhang et al., 2018) Meanwhile, high temperature brings about more decomposition of NO in the engine. The decomposition reaction of ^{14}NO occurs faster than that of ^{15}NO since NO decomposition reactions are usually dynamically controlled, which leads to enrichment of ^{15}NO and an increase in $\delta^{15}N–NO_x$ values.(Zong et al., 2020) This is to some extent consistent with our result that the mean values of $\delta^{15}N–NO_x$ emitted from the most powerful bulk carrier SH1 and the least powerful fishing vessel Y2 in this study are the largest and smallest among all sampled vessels, respectively, although they are influenced by many other factors. The minor influence of fuel type on $\delta^{15}N–NO_x$ values is due to the principle of thermally generated NO_x by internal combustion engines of ships as mentioned above.(Goldsworthy, 2003) The operational condition of ships has the least effect on the variation in $\delta^{15}N–NO_x$ values. Previous studies have also elucidated that $\delta^{15}N–NO_x$ values emitted from motor vehicles were mainly altered during the period of cold or hot start and vary within a narrow range after 2 or 3 min of cold or hot start. The three operating modes of ships in this study should all be the state after a cold or hot start, so the minimum effect of the operating mode on the $\delta^{15}N–NO_x$ values is in accordance with the observations of motor vehicles.(Walters et al., 2015a; Walters et al., 2015b; Zong et al., 2020)

Text S3. Significance of ship-emitted $\delta^{15}N–NO_x$ values for accurate source apportionment of NO_x

With the transformation of the energy structure and the improvement of environmental standards, NO_x emissions from power plants as well as residential coal combustion have been increasingly restricted, and transportation has become one of the most widely concerned emission sources of NO_x in the atmosphere in recent years.(Luo et al., 2019; Song et al., 2019; Zong et al., 2017) To assess the impact

of transportation NO_x sources, we integrated vehicle emissions from coastal China and ship emissions from offshore China in 2017 reported in previous studies (the data are available on the website of http://meicmodel.org) and made the combined emission inventory of NO_x from ships and vehicles.(Li et al., 2017; Liu et al., 2016) As shown in Figure S8, NO_x emissions are significantly higher in coastal areas, especially in some shipping-intensive ports in the Bohai Rim, Yangtze River Delta and Pearl River Delta, such as Qingdao, Shanghai and Guangzhou, indicating that the impact of ship emissions on atmospheric NO_x pollution cannot be ignored. In addition, it can be obtained in view of the previous analysis that the $\delta^{15}N$–NO_x values of ship and motor vehicle emissions are distinctly different. Therefore, reliable $\delta^{15}N$–NO_x values of ship emissions are essential for the accuracy of source apportionment when assessing atmospheric NO_x sources in coastal areas based on $\delta^{15}N$ methods.

Table S1. Technical parameters of the test ships

vessel ID	engine power (kW)	rated speed (rpm)	maximum design speed (knot)	cylinders	gross tonnage (ton)	emission standard	ship length × width (m)	auxiliary engines	fuel
SH1	15748	75	14.5	6	94674	Tier III	292 × 45	yes	residual oil and diesel
SH2	1470	850	11.52	6	6247	Tier II	109.8 × 26.8	yes	residual oil and diesel
SH3	138.4	1150	8.45	4	77	Tier I	24 × 5.01	no	diesel
SH4	120	1200	8	6	20	Tier II	28 × 4.8	yes	diesel
SH5	178	1500	7	6	300	Tier II	35 × 6	no	diesel
Y1	33	1500	7	4	5	Tier I	14 × 2.5	no	diesel
Y2	29	1800	7	4	3	before Tier I	12 × 4	no	diesel
K1	240	1900	20	6	30	Tier II	19.38 × 14.1	no	diesel
KK1	610	750	11	6	499	Tier II	48.7 × 9	yes	diesel

Table S2. Meteorological parameters during ship exhaust sampling (average values)

vessel ID	temperature (°C)	wind speed (m s^{-1})	relative humidity (%)	sampling area	sampling period
SH1	24	2.8	66	Shanghai Port	2020/09/12–16
SH2	1	4.5	51	Yantai Port	2020/01/11–12
SH3	25	4.3	55	Dongying Port	2020/09/22
SH4	27	3.0	68	Weihai Port	2020/08/21
SH5	1	5.1	49	Yantai Port	2020/01/15
Y1	27	3.0	68	Weihai Port	2020/08/21
Y2	26	2.9	65	Weihai Port	2020/08/22
K1	27	3.3	63	Dandong Port	2021/07/08
KK1	25	4.1	58	Yantai Port	2021/09/13

Table S3. Details on NO_x concentrations and $\delta^{15}N$–NO_x values for collected ship exhaust (actual emissions after integration of main engine and auxiliary engine)

vessel ID	operational status	NO_x (ppm)		$\delta^{15}N$ (‰)		n (replicates)
		ave	std	ave	std	
SH1	maneuvering	144.0	66.1	−7.4	0.1	4
	cruising	114.4	93.9	−8.1	6.0	12
	total	129.2	80.0	−7.8	3.0	16
SH2	maneuvering	186.2	37.0	−11.4	0.0	6
	cruising	147.3	68.0	−10.6	1.9	12
	total	166.8	52.5	−11.0	0.9	18
SH3	hoteling	342.0	213.8	−31.0	2.0	6
	maneuvering	338.4	143.4	−30.5	1.3	6
	cruising	314.3	170.0	−29.7	5.9	12
	total	331.6	175.8	−30.4	3.1	24
SH4	hoteling	73.4	0.3	−10.0	0.0	2
	cruising	68.0	9.9	−15.7	2.0	2
	total	70.7	5.1	−12.9	1.0	4
SH5	hoteling	197.5	34.3	−18.8	4.7	4
	maneuvering	236.6	80.0	−13.3	10.3	2
	cruising	169.9	71.3	−24.3	10.3	4
	total	201.3	61.9	−18.8	8.4	10
Y1	hoteling	197.3	104.7	−24.2	4.6	4
	maneuvering	348.3	21.9	−17.5	9.5	2
	cruising	230.9	56.3	−21.1	5.2	6
	total	258.8	61.0	−20.9	6.4	12
Y2	hoteling	95.5	19.6	−34.3	1.1	4
	maneuvering	134.0	14.0	−32.7	3.1	2
	cruising	84.9	24.0	−33.9	1.3	6
	total	104.8	19.2	−33.6	1.8	12
K1	hoteling	19.4	9.9	−11.3	0.7	6

	cruising	10.9	0.5	−8.4	2.5	4
	total	15.1	5.2	−9.9	1.6	10
KK1	hoteling	22.2	0.4	−12.4	0.0	4
	maneuvering	52.4	17.7	−12.4	0.0	4
	cruising	61.2	27.2	−11.4	0.7	10
	total	45.2	15.1	−12.1	0.2	18

Table S4. Statistics of $\delta^{15}N$–NO_x values and ranges of variation for emissions from other sources

source	time		sampling[a]		^{15}N (‰) ave	std	min	max	n (replicates)	ref	ave	std
vehicle exhaust		individual vehicle tailpipes without TWC	the standard gas bubbler (KOH solution)	NO_x	3.7	0.3	3.4	3.9	3	(Moore, 1977)	0.46	6.93
		individual vehicle tailpipes without TWC	10 L glass tube ($NaOH/H_2O_2$ solution)	NO_x	−1.8					(Freyer, 1978)		
		individual vehicle tailpipes without TWC	17 L glass or polythene container ($NaOH/H_2O_2$ solution)	NO_x	−7.0	4.7	−13	−2	8	(Heaton, 1990)		
	1994/04/29 –08/19	roadside	the denuder system (CrO_3/H_3PO_4 solid oxidizer + KOH/guaiacol coating)	NO	3.1	5.4	−5	9.5	9	(Ammann et al., 1999)		
			the denuder system (KOH/guaiacol coating)	NO_2	5.7	2.8	1.6	10.1	9			
	2008/07−11	roadside	the Ogawa sampler (14.5 mm TEA coating filter)	NO_2	1.0	3.5	−5.1	7.3		(Redling et al., 2013)		
			the HNO_3 sampler (PTFE membrane + 47 mm nylon filter)	HNO_3	2.8		−1	3.1				
	2010/05– 2011/05	outside and in the tunnel	the Ogawa sampler (14 mm TEA coating filter)	NO_2	15.0	1.6	10.2	17.0	22	(Felix and Elliott, 2014)		
			the HNO_3 sampler (2 μm 47 mm Teflon filter + 47 mm nylon filter)	HNO_3	5.7	2.8	0.9	11.1	15			
	2014/10/01 – 2015/05/01	individual vehicle tailpipes	evacuated 2 L borosilicate bottle (H_2SO_4/H_2O_2 solution)	NO_x	−11	6.62	−28.1	8.5	55	(Walters et al., 2015b)		
	2014/06/20	individual vehicle	evacuated 2 L	NO_x	−3.0	7.2	−23.3	10.5	78	(Walt		

	–09/26	tailpipes	borosilicate bottle (H_2SO_4/H_2O_2 solution)							ers et al., 2015a)		
	2015/03–08	roadside	the gas-washing bottle ($KMnO_4$/NaOH solution)	NO_x			−9	−2	78	(Miller et al., 2017)		
	2019/04/16–27	individual vehicle tailpipes	the gas-washing bottle ($KMnO_4$/NaOH solution)	NO_x	−8.66	5.34	−18.8	6.43	61	(Zong et al., 2020)		
biogenic soil emission	1998/11/05–18	fertilized soil + the dynamic chamber	the trapping system (a molecular sieve 5A trap)	N_2O			−46	5	15	(Perez et al., 2001)		
		fertilized soil + the dynamic flow-through chamber	the denuder system (CrO_3/H_3PO_4 solid oxidizer + KOH/guaiacol coating)	NO	−32.3		−48.9	−19.9	24	(Li and Wang, 2008)		
	2010/06/19–07/22; 2011/06/2–06/19	fertilized soil + the feedlot flux chamber	the Ogawa sampler (14 mm TEA coating filter)	NO_2	−28.7	2.2	−30.8	−26.5	2	(Felix and Elliott, 2013, 2014)	−33.65	5.55
		re-wetted soil	9.5 mm i.d., ca. 240 cm length Teflon tubing (O_3) + 500 mL gas washing bottle (TEA solution)	NO	−43.0	9.3	−59.8	−23.4	35	(Yu and Elliott, 2017)		
	2016/05; 2017/05–06	fertilized no-till soil + the dynamic flux chamber	the gas-washing bottle ($KMnO_4$/NaOH solution)	NO_x	−30.6 (emission-weighted)		−44.2	14.0	37	(Miller et al., 2018)		

biomass burning	fall of 2016	stack and chamber fires	250 mL gas-washing bottle ($KMnO_4$/NaOH solution)	NO_x	1.0	4.1	−7.2	12	24	(Fibiger and Hastings, 2016)	−0.78	4.69
			the Nylasorb filter	HNO_3	6.3							
		chamber fires	the gas-washing bottle ($KMnO_4$/NaOH solution)	NO_x	1.1	3.1	−4.3	7.0	14	(Chai et al., 2019)		
			the Teflon particulate filter	pNO_3^-	−8.9	1.3	−10.6	−7.4	5			
	autumn	rural cooking stoves and open burning	evacuated 2 L borosilicate bottle (H_2SO_4/H_2O_2 solution)	NO_x	−3.8	4.2	−11.9	3.1	42	(Shi et al., 2022)		
	November	stack fires (residential use)	the gas-washing bottle ($KMnO_4$/NaOH solution)	NO_x	−0.4	2.4	−5.6	3.2	21	(Zong et al., 2022)		
coal combustion		coal-fired power stations	NaOH/H_2O_2 solution	NO_x	9.6	2.9	6	13	5	(Heaton, 1990)	8.84	7.93
		thermal/prompt NO_x		NO	−6.2	0.9				(Snape et al., 2003)		
	2009/05–2011/04	coal-fired power plants (in stack)	evacuated and purged flask (H_2SO_4/H_2O_2 solution) / NaOH/H_2O_2 solution	NO_x	14.6	4.5	9.0	25.6	38	(Felix et al., 2012)		
	2009/12/08		TEA solution	NO_2	10.1	0.6	9.5	10.7	4			
	November	residential coal combustion	the gas-washing bottle ($KMnO_4$/NaOH solution)	NO_x	16.1	3.3	11.7	19.7	7	(Zong et al., 2022)		

[a]The full names of the abbreviated forms and chemical formulas mentioned in the table are as follows: three-way catalytic (TWC), potassium hydroxide (KOH), sodium hydroxide (NaOH), hydrogen peroxide (H_2O_2), chromium trioxide (CrO_3), phosphoric acid (H_3PO_4), triethanolamine (TEA), nitric acid (HNO_3), poly tetra fluoroethylene (PTFE), sulfuric acid (H_2SO_4), potassium permanganate ($KMnO_4$), ozone (O_3).

Table S5. Results of variance analysis

classification indicators	degree of freedom	sum of squares	mean of squares	F values	p (>F)
vessel category	3	3644	1214.5	19.343	3.30E−10
emission regulation	2	3070	1534.8	24.444	1.46E−09
fuel type	1	138	138.4	2.205	0.1403
operational status	2	380	189.9	3.025	0.0525

Table S6. The accuracy of methods implemented to evaluate the impact degree of different factors on the variation in ship-emitted $\delta^{15}N–NO_x$ values

	mean error	root mean squared error	mean absolute error	mean percentage error	mean absolute percentage error
ctree	−1.61E−15	6.333	4.490	−21.806	53.884
cforest	−0.052	5.798	4.300	−19.875	49.085
rpart	−1.61E−15	6.333	4.490	−21.806	53.884
random forest	−0.071	4.358	2.934	−8.955	29.870

Table S7. Mass-weighted $\delta^{15}N–NO_x$ values (‰) emitted from ships between 2001 and 2021

year	mean	standard deviation	lower quartiles	upper quartiles
2001	−33.52	0.57	−33.90	−33.14
2002	−33.03	0.73	−33.49	−32.56
2003	−32.91	0.79	−33.42	−32.39
2004	−32.66	0.82	−33.16	−32.14
2005	−32.16	0.98	−32.77	−31.50
2006	−32.09	1.01	−32.73	−31.42
2007	−31.84	1.05	−32.53	−31.14
2008	−31.62	1.05	−32.32	−30.91
2009	−31.26	1.11	−32.04	−30.49
2010	−31.00	1.12	−31.74	−30.25
2011	−30.92	1.16	−31.66	−30.15
2012	−30.77	1.17	−31.53	−30.00
2013	−29.38	1.25	−30.17	−28.55
2014	−28.67	1.21	−29.43	−27.90
2015	−27.68	1.26	−28.45	−26.83
2016	−27.89	1.21	−28.65	−27.08
2017	−27.76	1.21	−28.50	−26.95
2018	−27.45	1.23	−28.20	−26.63
2019	−27.07	1.25	−27.85	−26.29
2020	−26.31	1.34	−27.16	−25.43
2021	−25.60	1.44	−26.49	−24.68
2022	−24.24	1.49	−25.19	−23.30

2023	−23.42	1.40	−24.41	−22.47
2024	−23.04	1.46	−24.02	−22.10
2025	−22.45	1.53	−23.54	−21.46
2026	−22.10	1.52	−23.13	−21.11
2027	−20.33	1.52	−21.40	−19.30
2028	−20.15	1.55	−21.22	−19.12
2029	−20.28	1.69	−21.41	−19.15
2030	−18.87	1.65	−20.01	−17.77
2031	−17.68	1.70	−18.89	−16.55
2032	−17.60	1.73	−18.72	−16.45
2033	−17.50	1.64	−18.56	−16.45
2034	−16.69	1.67	−17.80	−15.60
2035	−15.57	1.69	−16.75	−14.48
2036	−14.09	1.69	−15.16	−12.95
2037	−13.76	1.68	−14.92	−12.60
2038	−12.52	1.67	−13.74	−11.39
2039	−11.70	1.73	−12.87	−10.55
2040	−10.09	1.72	−11.30	−8.87
2041	−9.79	1.80	−11.06	−8.55
2042	−9.26	1.82	−10.60	−7.99
2043	−9.30	1.76	−10.55	−8.09
2044	−8.84	1.91	−10.07	−7.53
2045	−8.58	1.92	−9.87	−7.26
2046	−8.09	1.95	−9.44	−6.75
2047	−8.23	1.94	−9.50	−6.99
2048	−8.10	1.94	−9.46	−6.75
2049	−8.06	1.96	−9.32	−6.71
2050	−8.10	2.01	−9.54	−6.77
2051	−8.06	1.96	−9.33	−6.74
2052	−8.17	2.02	−9.52	−6.92

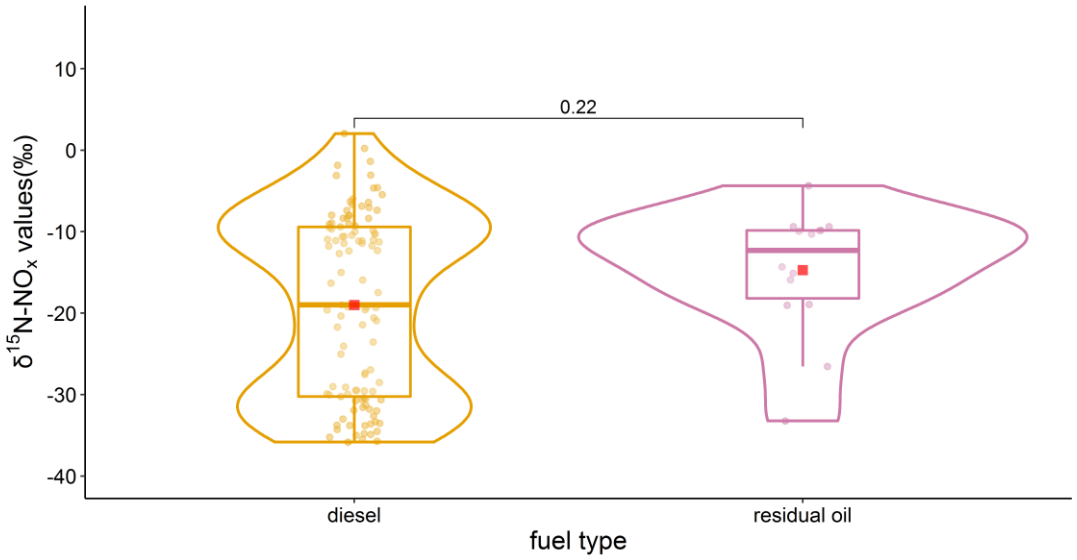

Figure S1. $\delta^{15}N–NO_x$ values emitted from ships grouped by different fuels. (red square, mean; center line, median; box bounds, upper and lower quartiles; whiskers, 1.5 times interquartile range; points, outliers; outer line, data distribution). The p value indicating the distinction between two selected groups is marked on the upper of the panel (the Mann–Whitney U test).

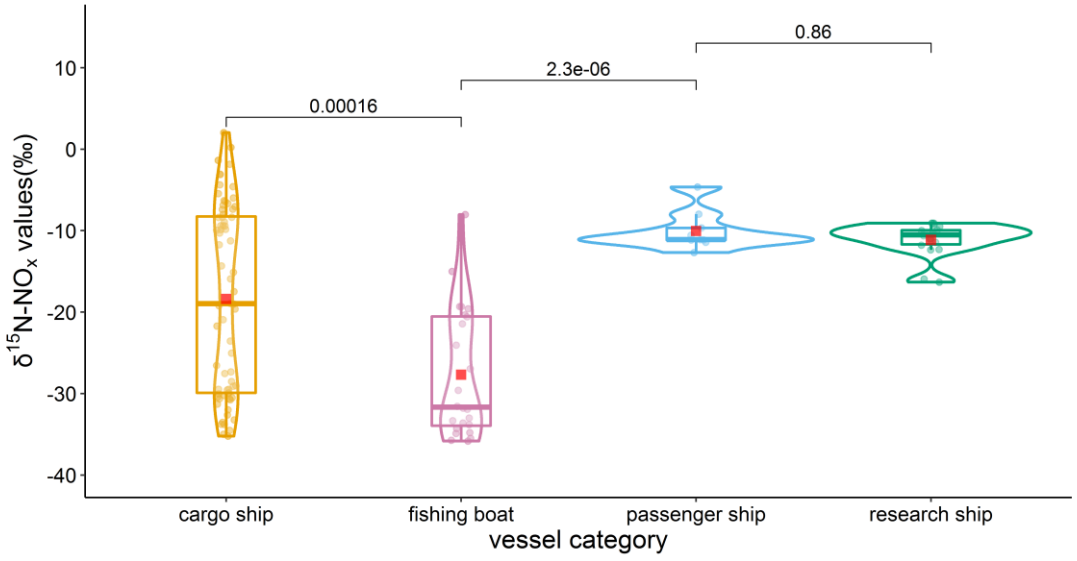

Figure S2. $\delta^{15}N–NO_x$ values emitted from ships grouped by different ship categories. (red square, mean; center line, median; box bounds, upper and lower quartiles; whiskers, 1.5 times interquartile range; points, outliers; outer line, data distribution). The p values indicating the distinction between two selected groups are marked on the upper of the panel (the Mann–Whitney U test).

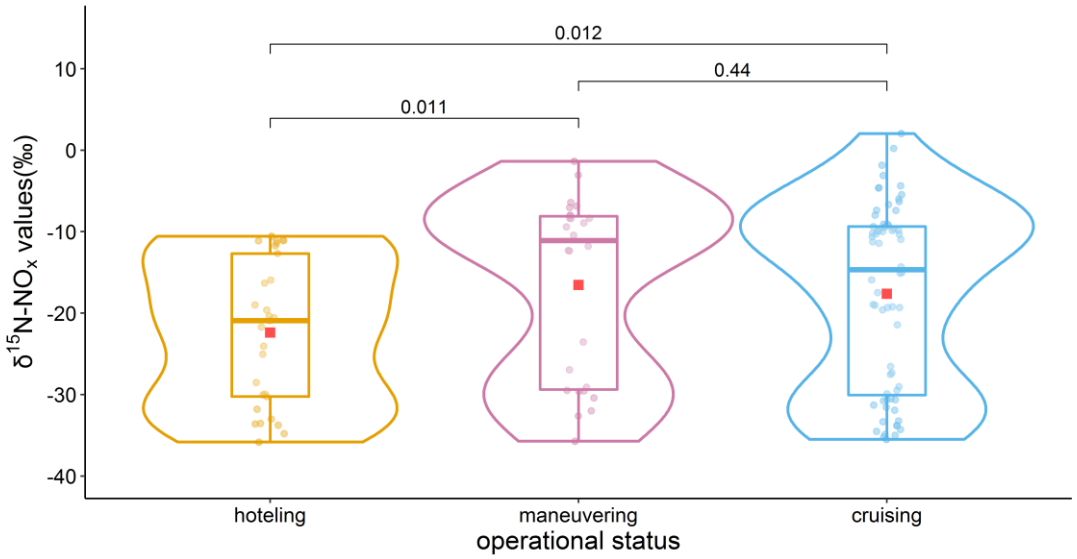

Figure S3. $\delta^{15}N–NO_x$ values emitted from ships grouped by different operational statuses. (red square, mean; center line, median; box bounds, upper and lower quartiles; whiskers, 1.5 times interquartile range; points, outliers; outer line, data distribution). The p values indicating the distinction between two selected groups are marked on the upper of the panel (the Mann–Whitney U test).

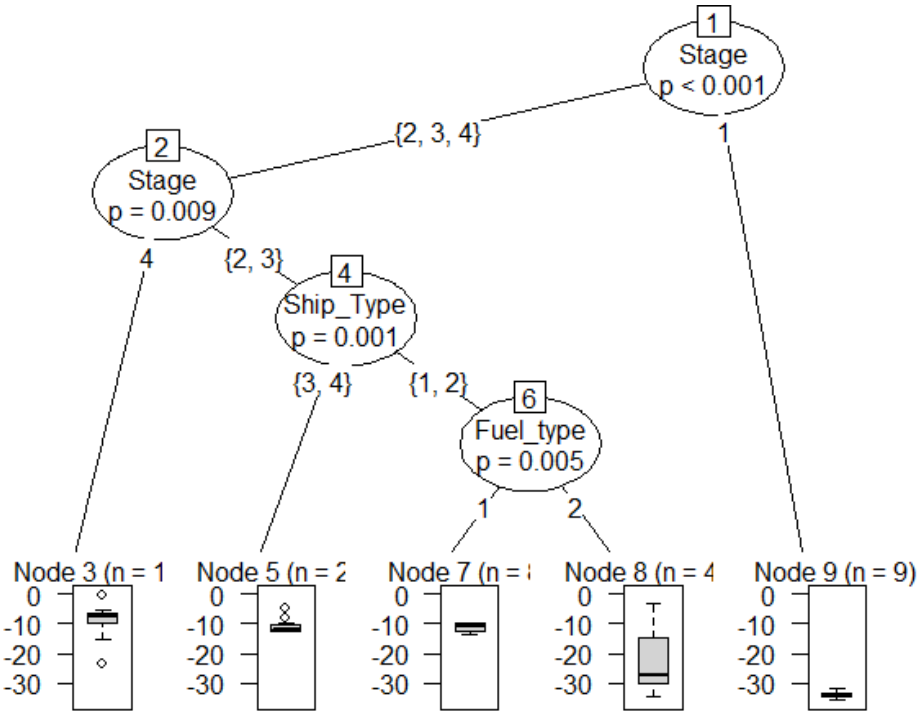

Figure S4. Conditional inference trees (CIT) for the $\delta^{15}N–NO_x$ values emitted from ships. For each inner node, the p values are given and the range of $\delta^{15}N–NO_x$ values is displayed for each terminal node.

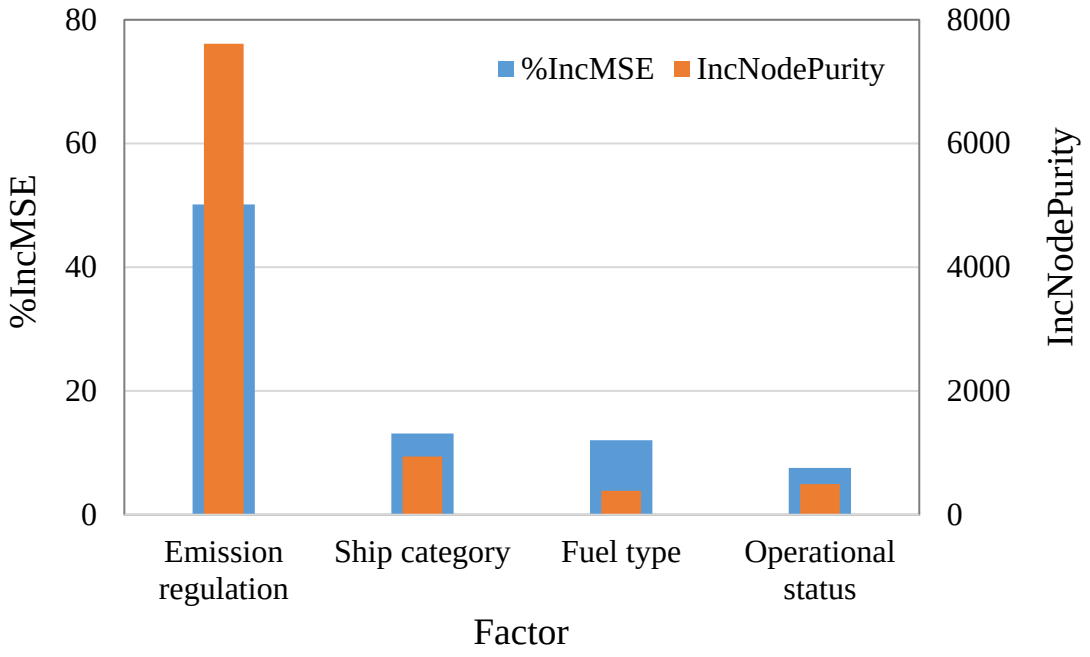

Figure S5. Increase in mean squared error (%IncMSE) and increase in node purity (IncNodePurity) of selected factors for the $\delta^{15}N–NO_x$ values from ships calculated by random forest (RF).

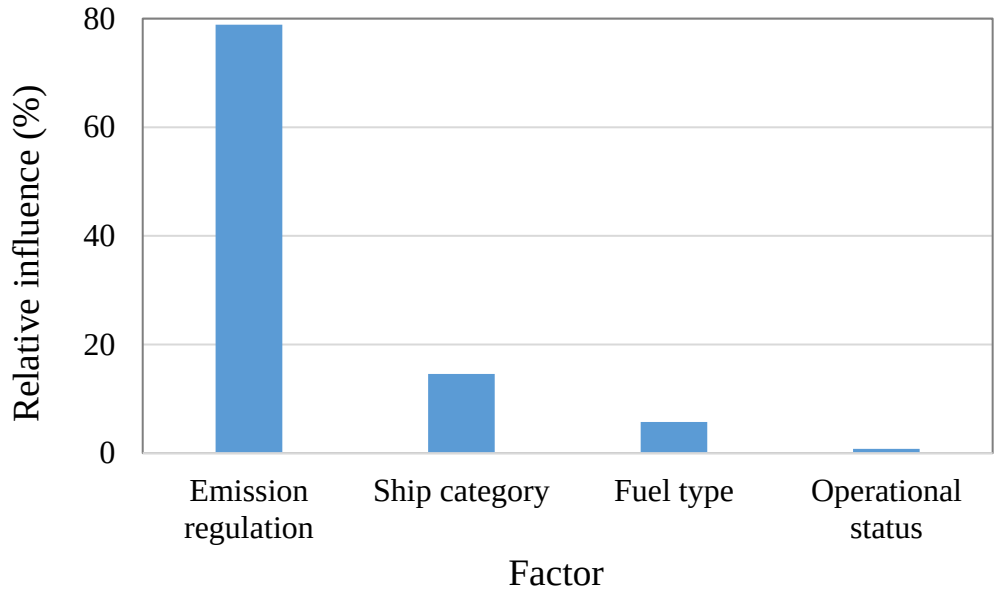

Figure S6. Relative influence (%) of four selected factors on $\delta^{15}N–NO_x$ values from ships calculated by boosted regression trees (BRT).

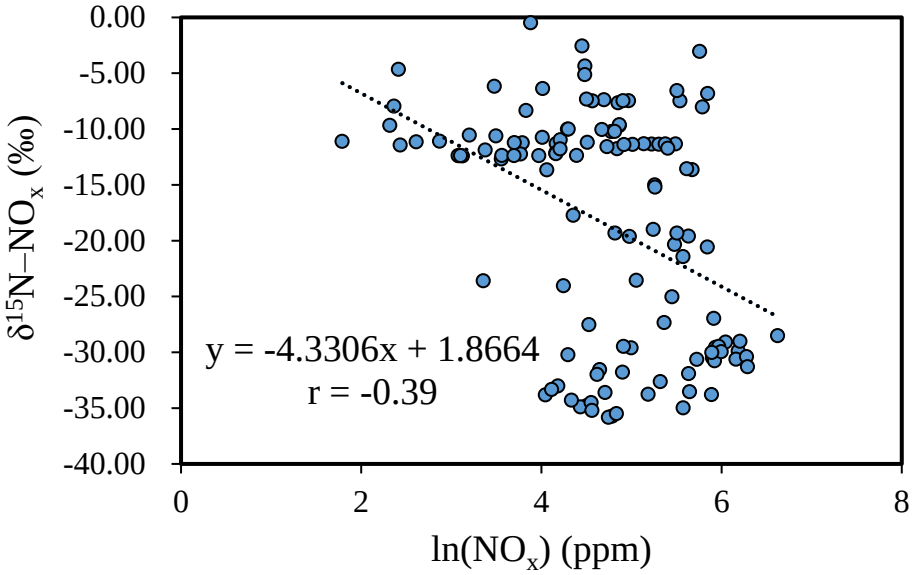

Figure S7. The negative logarithmic relationship between $\delta^{15}N–NO_x$ values and NO_x concentration emitted from ships.

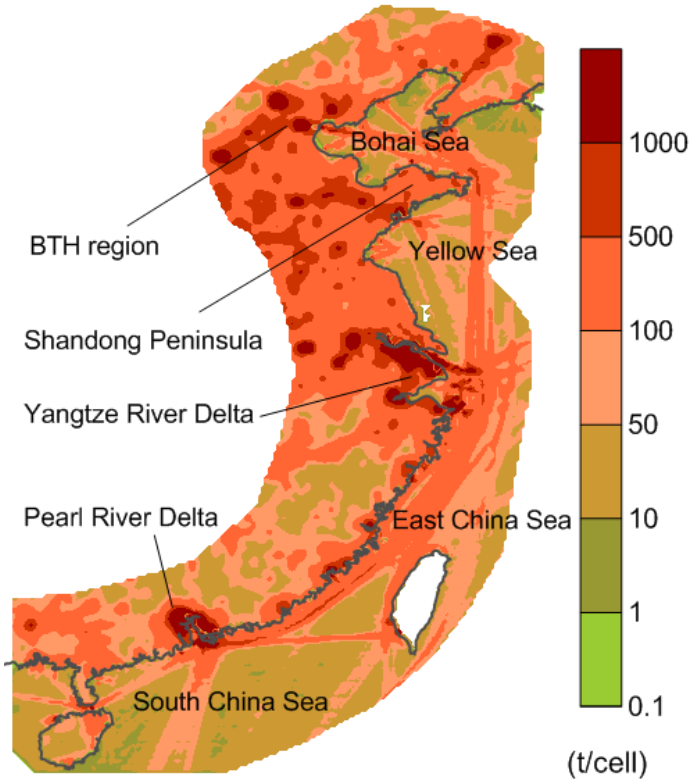

Figure S8. Spatial distribution of annual NO_x emissions from coastal vehicles and offshore ships in China in 2017 (a horizontal resolution of 0.1° × 0.1° latitude/longitude).

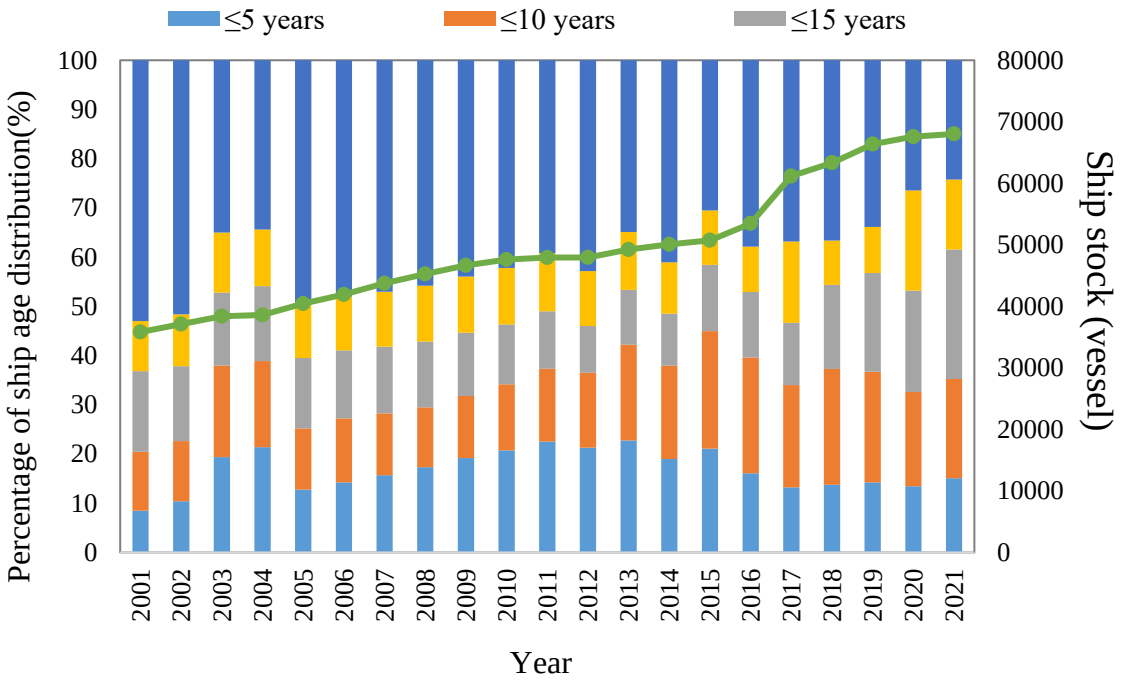

Figure S9. The age distribution of ships larger than 300 gross tonnage (GT) in the international merchant fleet during 2001 and 2021.

References

Ammann, M., Siegwolf, R., Pichlmayer, F., Suter, M., Saurer, M., and Brunold, C.: Estimating the uptake of traffic-derived NO_2 from ^{15}N abundance in Norway spruce needles, Oecologia, 118, 124-131, https://doi.org/10.1007/s004420050710, 1999.

Chai, J., Miller, D. J., Scheuer, E., Dibb, J., Selimovic, V., Yokelson, R., Zarzana, K. J., Brown, S. S., Koss, A. R., Warneke, C., and Hastings, M.: Isotopic characterization of nitrogen oxides (NO_x), nitrous acid (HONO), and nitrate (pNO_3^-) from laboratory biomass burning during FIREX, Atmos. Meas. Tech., 12, 6303-6317, https://doi.org/10.5194/amt-12-6303-2019, 2019.

Elith, J., Leathwick, J. R., and Hastie, T.: A working guide to boosted regression trees, J. Anim. Ecol., 77, 802-813, https://doi.org/10.1111/j.1365-2656.2008.01390.x, 2008.

Felix, J. D., Elliott, E. M., and Shaw, S. L.: Nitrogen isotopic composition of coal-fired power plant NO_x: Influence of emission controls and implications for global emission inventories, Environ. Sci. Technol., 46, 3528-3535, https://doi.org/10.1021/es203355v, 2012.

Felix, J. D. and Elliott, E. M.: The agricultural history of human-nitrogen interactions as recorded in ice core δN^{15}-NO_3^-, Geophys. Res. Lett., 40, 1642-1646, https://doi.org/10.1002/grl.50209, 2013.

Felix, J. D. and Elliott, E. M.: Isotopic composition of passively collected nitrogen dioxide emissions: Vehicle, soil and livestock source signatures, Atmos. Environ., 92, 359-366, https://doi.org/10.1016/j.atmosenv.2014.04.005, 2014.

Fibiger, D. L. and Hastings, M. G.: First measurements of the nitrogen isotopic composition of NO_x from biomass burning, Environ. Sci. Technol., 50, 11569-11574, https://doi.org/10.1021/acs.est.6b03510, 2016.

Freyer, H. D.: Seasonal trends of NH_4^+ and NO_3^- nitrogen isotope composition in rain collected at Julich, Germany, Tellus, 30, 83-92, https://doi.org/10.1111/j.2153-3490.1978.tb00820.x, 1978.

Goldsworthy, L.: Reduced kinetics schemes for oxides of nitrogen emissions from a slow-speed marine diesel engine, Energy Fuel., 17, 450-456, https://doi.org/10.1021/ef020172c, 2003.

Heaton, T. H. E.: $^{15}N/^{14}N$ ratios of NO_x from vehicle engines and coal-fired power stations, Tellus B, 42, 304-307, https://doi.org/10.1034/j.1600-0889.1990.t01-1-00009.x, 1990.

Hothorn, T., Hornik, K., and Zeileis, A.: Unbiased recursive partitioning: A conditional inference framework, J. Comput. Graph. Stat., 15, 651-674, https://doi.org/10.1198/106186006x133933, 2006.

Kruskal, W. H. and Wallis, W. A.: Use of Ranks in One-Criterion Variance Analysis, J. Am. Stat. Assoc., 47, 583-621, https://doi.org/10.1080/01621459.1952.10483441, 1952.

Li, D. and Wang, X.: Nitrogen isotopic signature of soil-released nitric oxide (NO) after fertilizer application, Atmos. Environ., 42, 4747-4754, https://doi.org/10.1016/j.atmosenv.2008.01.042, 2008.

Li, M., Liu, H., Geng, G. N., Hong, C. P., Liu, F., Song, Y., Tong, D., Zheng, B., Cui, H. Y., Man, H. Y., Zhang, Q., and He, K. B.: Anthropogenic emission inventories in China: a review, Natl. Sci. Rev., 4, 834-866, https://doi.org/10.1093/nsr/nwx150, 2017.

Liu, H., Fu, M., Jin, X., Shang, Y., Shindell, D., Faluvegi, G., Shindell, C., and He, K.: Health and climate impacts of ocean-going vessels in East Asia, Nat. Clim. Change, 6, 1037-+, https://doi.org/10.1038/nclimate3083, 2016.

Luo, L., Wu, Y., Xiao, H., Zhang, R., Lin, H., Zhang, X., and Kao, S.-j.: Origins of aerosol nitrate in Beijing during late winter through spring, Sci. Total Environ., 653, 776-782, https://doi.org/10.1016/j.scitotenv.2018.10.306, 2019.

Mann, H. B. and Whitney, D. R.: On a test of whether one of two random variables is stochastically larger than the other, Ann. Math. Stat., 50-60, 1947.

Miller, D. J., Wojtal, P. K., Clark, S. C., and Hastings, M. G.: Vehicle NO_x emission plume isotopic signatures: Spatial variability across the eastern United States, J. Geophys. Res.-Atmos., 122, 4698-4717, https://doi.org/10.1002/2016jd025877, 2017.

Miller, D. J., Chai, J., Guo, F., Dell, C. J., Karsten, H., and Hastings, M. G.: Isotopic composition of in situ soil NO_x emissions in manure-fertilizes cropland, Geophys. Res. Lett., 45, 12058-12066, https://doi.org/10.1029/2018gl079619, 2018.

Moore, H.: Isotopic composition of ammonia, nitrogen-dioxide and nitrate in atmosphere, Atmos. Environ., 11, 1239-1243, https://doi.org/10.1016/0004-6981(77)90102-0, 1977.

Perez, T., Trumbore, S. E., Tyler, S. C., Matson, P. A., Ortiz-Monasterio, I., Rahn, T., and Griffith, D. W. T.: Identifying the agricultural imprint on the global N_2O budget using stable isotopes, J. Geophys. Res.-Atmos., 106, 9869-9878, https://doi.org/10.1029/2000jd900809, 2001.

Redling, K., Elliott, E., Bain, D., and Sherwell, J.: Highway contributions to reactive nitrogen deposition: tracing the fate of vehicular NO_x using stable isotopes and plant biomonitors, Biogeochemistry, 116, 261-274, https://doi.org/10.1007/s10533-013-9857-x, 2013.

Shi, Y., Tian, P., Jin, Z., Hu, Y., Zhang, Y., and Li, F.: Stable nitrogen isotope composition of NO_x of biomass burning in China, Sci. Total Environ., 803, 149857, https://doi.org/10.1016/j.scitotenv.2021.149857, 2022.

Snape, C. E., Sun, C. G., Fallick, A. E., Irons, R., and Haskell, J.: Potential of stable nitrogen isotope ratio measurements to resolve fuel and thermal NO_x in coal combustion, Abstr. Pap. Am. Chem. Soc., 225, U843-U843, 2003.

Song, W., Wang, Y.-L., Yang, W., Sun, X.-C., Tong, Y.-D., Wang, X.-M., Liu, C.-Q., Bai, Z.-P., and Liu, X.-Y.: Isotopic evaluation on relative contributions of major NO_x sources to nitrate of $PM_{2.5}$ in Beijing, Environ. Pollut., 248, 183-190, https://doi.org/10.1016/j.envpol.2019.01.081, 2019.

Speybroeck, N.: Classification and regression trees, Int. J. Public Health, 57, 243-246, https://doi.org/10.1007/s00038-011-0315-z, 2012.

Strobl, C., Boulesteix, A.-L., Zeileis, A., and Hothorn, T.: Bias in random forest variable importance measures: Illustrations, sources and a solution, BMC Bioinformatics, 8, https://doi.org/10.1186/1471-2105-8-25, 2007.

Walters, W. W., Goodwin, S. R., and Michalski, G.: Nitrogen stable isotope composition ($\delta^{15}N$) of vehicle-emitted NO_x, Environ. Sci. Technol., 49, 2278-2285, https://doi.org/10.1021/es505580v, 2015a.

Walters, W. W., Tharp, B. D., Fang, H., Kozak, B. J., and Michalski, G.: Nitrogen isotope composition of thermally produced NO_x from various fossil-fuel combustion sources, Environ. Sci. Technol., 49, 11363-11371, https://doi.org/10.1021/acs.est.5b02769, 2015b.

Yu, Z. and Elliott, E. M.: Novel method for nitrogen isotopic analysis of soil-emitted nitric oxide, Environ. Sci. Technol., 51, 6268-6278, https://doi.org/10.1021/acs.est.7b00592, 2017.

Zhang, F., Chen, Y., Chen, Q., Feng, Y., Shang, Y., Yang, X., Gao, H., Tian, C., Li, J., Zhang, G., Matthias, V., and Xie, Z.: Real-world emission factors of gaseous and particulate pollutants from marine fishing boats and their total emissions in China, Environ. Sci. Technol., 52, 4910-4919, https://doi.org/10.1021/acs.est.7b04002, 2018.

Zong, Z., Wang, X., Tian, C., Chen, Y., Fang, Y., Zhang, F., Li, C., Sun, J., Li, J., and Zhang, G.: First assessment of NO_x sources at a regional background site in North China using isotopic analysis linked with modeling, Environ. Sci. Technol., 51, 5923-5931, https://doi.org/10.1021/acs.est.6b06316, 2017.

Zong, Z., Sun, Z., Xiao, L., Tian, C., Liu, J., Sha, Q., Li, J., Fang, Y., Zheng, J., and Zhang, G.: Insight

into the variability of the nitrogen isotope composition of vehicular NO_x in China, Environ. Sci. Technol., 54, 14246-14253, https://doi.org/10.1021/acs.est.0c04749, 2020.

Zong, Z., Shi, X., Sun, Z., Tian, C., Li, J., Fang, Y., Gao, H., and Zhang, G.: Nitrogen isotopic composition of NO_x from residential biomass burning and coal combustion in North China, Environ. Pollut., 304, 119238-119238, https://doi.org/10.1016/j.envpol.2022.119238, 2022.